Stabilization of Liner Implosions via a Dynamic Screw Pinch

Paul C. Campbell,[1] T. M. Jones,[1] J. M. Woolstrum,[1] N. M. Jordan,[1] P. F. Schmit,[2] J. B. Greenly,[3] W. M. Potter,[3] E. S. Lavine,[3] B. R. Kusse,[3] D. A. Hammer,[3] and R. D. McBride[1]

[1]*Nuclear Engineering and Radiological Sciences, University of Michigan, Ann Arbor, Michigan 48109, USA*
[2]*Sandia National Laboratories, Albuquerque, New Mexico 87185, USA*
[3]*Laboratory of Plasma Studies, Cornell University, Ithaca, New York 14853, USA*

(Received 11 September 2019; revised 12 May 2020; accepted 9 June 2020; published 16 July 2020)

Magnetically driven implosions are susceptible to magnetohydrodynamic instabilities, including the magneto-Rayleigh-Taylor instability (MRTI). To reduce MRTI growth in solid-metal liner implosions, the use of a dynamic screw pinch (DSP) has been proposed [P. F. Schmit *et al.*, Phys. Rev. Lett. **117**, 205001 (2016)]. In a DSP configuration, a helical return-current structure surrounds the liner, resulting in a helical magnetic field that drives the implosion. Here, we present the first experimental tests of a solid-metal liner implosion driven by a DSP. Using the 1-MA, 100–200-ns COBRA pulsed-power driver, we tested three DSP cases (with peak axial magnetic fields of 2 T, 14 T, and 20 T) and a standard z-pinch (SZP) case (with a straight return-current structure and thus zero axial field). The liners had an initial radius of 3.2 mm and were made from 650-nm-thick aluminum foil. Images collected during the experiments reveal that helical MRTI modes developed in the DSP cases, while nonhelical (azimuthally symmetric) MRTI modes developed in the SZP case. Additionally, the MRTI amplitudes for the 14-T and 20-T DSP cases were smaller than in the SZP case. Specifically, when the liner had imploded to half of its initial radius, the MRTI amplitudes for the SZP case and for the 14-T and 20-T DSP cases were, respectively, 1.1 ± 0.3 mm, 0.7 ± 0.2 mm, and 0.3 ± 0.1 mm. Relative to the SZP, the stabilization obtained using the DSP agrees reasonably well with theoretical estimates.

DOI: 10.1103/PhysRevLett.125.035001

Fast z-pinch implosions [1,2] are used to study radiation generation [3,4], material properties [5,6], laboratory astrophysics [7,8], and inertial confinement fusion (ICF)—e.g., Magnetized Liner Inertial Fusion (MagLIF) on the 25-MA, 100-ns Z facility at Sandia National Laboratories, where a thick metal tube (or "liner") is imploded to compress preheated and premagnetized fusion fuel [9–12]. Z-pinch implosions are, however, susceptible to magnetohydrodynamic (MHD) instabilities (MHDI), such as the sausage instability, the kink instability, higher-order helical instabilities in general, and the magneto-Rayleigh-Taylor (MRT) instability (MRTI) [13–20]. The fastest growing instability modes are those which satisfy $\mathbf{k} \cdot \mathbf{B} = 0$, where $\mathbf{k}$ is the wave vector of the instability and $\mathbf{B}$ is the driving magnetic field. These modes are the fastest growing modes because they are not affected by the stabilizing influence of magnetic tension. Thus, in a standard z-pinch (SZP) configuration, where an axial current density J_z induces an azimuthal magnetic field B_θ, the fastest growing modes are azimuthally symmetric (azimuthal mode number $m = 0$).

In fast z-pinch implosions, various techniques are applied to control the deleterious effects of MHDI. In MagLIF, for example, thick liner walls are used to prevent MHDI from feeding through the liner wall and perturbing the fusion fuel contained inside. An important parameter for characterizing the liner's susceptibility to MHDI feedthrough is the liner's initial aspect ratio, $A_{r0} \equiv r_{\ell 0}/\delta_{\ell 0}$, where $r_{\ell 0}$ is the initial radius of the liner's outer surface, and $\delta_{\ell 0}$ is the liner's initial wall thickness. MagLIF liners on the Z facility typically use $A_{r0} \approx 6$, where $r_{\ell 0} \approx 3$ mm, and $\delta_{\ell 0} \approx 500$ μm; larger A_{r0} liners are more susceptible to MHDI feedthrough, while lower A_{r0} liners result in slower implosion velocities. Similarly, experiments designed to study dynamic material properties use low aspect-ratio liners ($A_{r0} \approx 2$–4) to mitigate MHDI feedthrough and maintain sample uniformity under compression [5,6]. For the low-A_{r0} liners used on the Z facility, the wall thickness is greater than the electrical skin depth, $\delta_e \sim 100$ μm. Thus, the MHDI initially forms near the liner's outer surface and works its way toward the liner's inner surface throughout the implosion [21].

Instability development can also be influenced by an axial magnetic field. In SZP-driven MagLIF, for example, an external field coil system generates a spatially uniform $B_{z0} \approx 10$–20 T prior to the implosion. During the implosion, B_z in the fuel is amplified to >1000 T via flux compression. The amplified B_z insulates the hot fuel from the cold liner wall and traps charged fusion products in the fuel [22]. In SZP-driven MagLIF, B_z does not contribute to driving the implosion, but it does affect the development of MHDI. In experiments conducted with $B_{z0} \approx 10$ T, penetrating radiography revealed that helical instability modes developed with $m \approx 6$ and helical pitch angles of

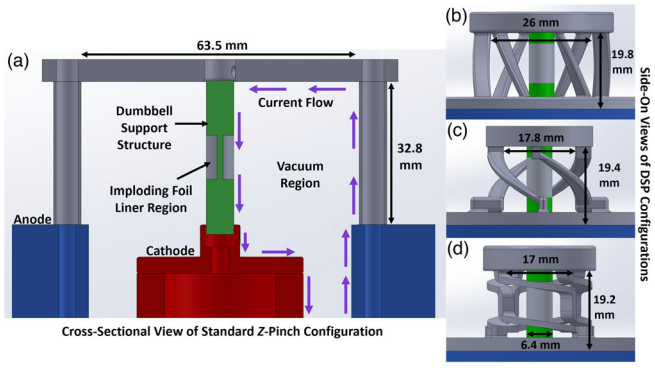

FIG. 1. CAD models of the return-current structures tested in these experiments. (a) Straight SZP return-current structure, including an illustration of the power feed. (b)–(d) Twisted DSP return-current structures, with predicted peak axial fields of 2 T, 14 T, and 20 T, respectively.

approximately 30° at an implosion convergence ratio $[C_r \equiv r_{\rm in}(0)/r_{\rm in}(t)]$ of approximately 7 [23]. These experiments were found to have less instability feedthrough than experiments conducted without an applied B_z field, where only nonhelical (azimuthally symmetric) instability modes were observed [21,24].

Liner stability has been further improved by the application of a thin dielectric coating to the liner's outer surface [25,26]. This was done to mitigate electrothermal and electrochoric instabilities (ETI and ECI [27]), which are thought to provide the initial seed for MHDI.

To further improve the stability of metal liner implosions, the use of a dynamic screw pinch (DSP) has been proposed and studied numerically [28]. Previously, this technique was used to stabilize gas-puff z-pinch implosions [29]. The DSP is generated using a helical (or "twisted") return-current structure, which surrounds the imploding liner, rather than the straight return-current structure of a SZP (see Fig. 1). The azimuthal component of the helical return-current path induces a $B_z(t)$ and a $J_\theta(t)$ at the liner's outer surface. Therefore, the net current density and magnetic field at the liner's outer surface are both helical—i.e., $\mathbf{J}(t) = J_\theta(t)\hat{\boldsymbol{\theta}} + J_z(t)\hat{\mathbf{z}}$ and $\mathbf{B}(t) = B_\theta(t)\hat{\boldsymbol{\theta}} + B_z(t)\hat{\mathbf{z}}$, where $B_\theta(t) \approx \mu_0 I(t)/[2\pi r_\ell(t)]$ and $B_z(t) \approx \mu_0 n I(t)$, and where n is the number of turns per unit length of the return-current structure. The implosion is driven by the total magnetic pressure at the liner's outer surface, $p_{\rm mag} = (B_\theta^2 + B_z^2)/(2\mu_0)$. The ratio B_z/B_θ will remain fixed until the liner starts to implode. During the implosion, $B_\theta(t) \propto I(t)/r_\ell(t)$ increases relative to $B_z(t) \propto I(t)$. This dynamically rotates the pitch angle of the driving magnetic field $\phi_B(t) = \arctan[B_z(t)/B_\theta(t)] = \arctan[2\pi n r_\ell(t)]$, with $\mathbf{B}(t)$ approaching a pure azimuthal field as $r_\ell(t)$ approaches the cylindrical axis. The rotating magnetic field thus drives a spectrum of modes (and azimuthal mode numbers) with $\mathbf{k}\cdot\mathbf{B} = 0$ satisfied at some point during the implosion; however, this also reduces the overall duration that any one mode is driven with $\mathbf{k}\cdot\mathbf{B} = 0$ satisfied. By contrast, in a SZP configuration, $\mathbf{k}\cdot\mathbf{B} = 0$ is satisfied throughout the entire implosion for one and only one azimuthal mode number: $m = 0$. The linear perturbation analysis presented in Ref. [28] suggests that by $C_r \approx 4$–8, the cumulative exponential growth for a DSP-driven implosion could be 1 to 2 orders of magnitude less than that of a SZP-driven implosion for single modes with a final perturbation wavelength magnitude of 200–400 μm.

The DSP provides additional benefits beyond enhanced stability. For example, for the same generator current delivered to the liner (i.e., the same J_z and B_θ along the liner's outer surface), a DSP-driven MagLIF implosion could reach stagnation about 10 ns earlier than a SZP-driven MagLIF implosion, due to the additional magnetic pressure from the induced J_θ and B_z along the liner's outer surface [28]. Alternatively, for the same implosion time, the DSP can drive a liner with a larger initial radius and thus impart more kinetic energy into the imploding shell [29]. Furthermore, calculations suggest that the DSP configuration could be used to inject axial magnetic field into the MagLIF fuel, potentially removing the need for external B_z coils [30].

To study the physics of MagLIF-relevant liner implosions on 1-MA, 100-ns facilities, thin-foil liners are typically used. This is because 1-MA, 100-ns facilities lack the energy to implode massive, thick-walled MagLIF liners. The use of thin foils allows a liner with $r_{\ell 0} \sim 3$ mm to be imploded in ~100 ns (a MagLIF-relevant implosion trajectory). Since MRTI growth is governed by the acceleration history of the implosion [13], a MagLIF-relevant implosion trajectory should result in MagLIF-relevant MRTI growth. Indeed, previous thin-foil experiments have demonstrated relevancy to MagLIF. For example, thin-foil experiments at 650 kA have found both $m \approx 0$ instability structures for SZP cases with no applied axial field and more stable $m \approx 2$ helical structures for SZP cases with an externally applied $B_{z0} \approx 2$ T [31,32]. Note that with $\delta_{\ell 0} \sim 500$ nm, these thin foils should be highly susceptible to instability feedthrough ($A_{r0} \sim 6000$). However, because $\delta_e \gg \delta_{\ell 0}$ (initially), ohmic heating causes the thin foils to rapidly expand to $\delta_w \sim 100$–1000 μm prior to the implosion [33,34], thus lowering the *effective* A_{r0} to 3–30.

In this Letter, we present results from the first experimental tests of an initially solid-metal liner implosion driven by a DSP. The experiments were conducted on the 1-MA COBRA facility [35] using both short and long pulse modes (see Fig. 2). For these experiments, one straight return-current structure and three different helical return-current structures were tested (see Fig. 1). Despite their helicity, the twisted return-current structures had inductance values similar to that of the straight return-current structure (≈8 nH), because the straight structure was both taller and wider than the twisted structures. The twisted structures were 3D printed using a binder jetting process.

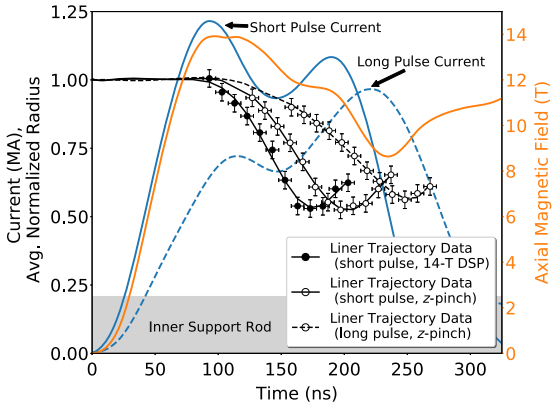

FIG. 2. Example experimental data, including drive currents, liner implosion trajectories, and the axial magnetic field, $B_z(t)$, measured on the mid-field DSP shot that produced the short-pulse current trace shown. Fitting curves for the experimentally measured liner radii are also plotted.

The liners were made from 650-nm-thick aluminum foils. The initial liner radius was 3.175 mm for all cases. Because the foils are so thin, the liners are not self-supporting. Thus, following Ref. [36], the liner loads were assembled by wrapping rectangular foils onto a plastic dumbbell-shaped support structure (see Fig. 1). The ends of the dumbbell have a diameter that matches the desired initial diameter of the liner, while the connecting rod in the central portion of the dumbbell has a diameter that is made as small as possible to allow as much implosion convergence as possible. For our experiments, the central portion of the dumbbell (the on-axis support rod) had a radius of 0.65 mm, allowing for a convergence ratio of up to 4.9. However, the maximum convergence ratio observed in our experiments (for the liner's outer surface) was approximately 2. The thin foils are not nearly as robust as the freestanding liners used in MagLIF experiments on Z. They are easily crinkled, resulting in larger seed perturbation amplitudes. Furthermore, there is a thin seam where the rectangular foil, wrapped into a cylindrical shell, overlaps itself. This seam was positioned azimuthally to minimize interference with imaging diagnostics and instability measurements.

The drive current was measured using a Rogowski coil in COBRA's power feed. The axial magnetic fields generated by the twisted return-current structures were measured using a micro B-dot probe [37] placed 3 mm radially outward from the liner surface. Examples of these measurements are presented in Fig. 2. Throughout these experiments, the rising edge of the $B_z(t)$ waveforms followed the rising edge of the drive current waveforms very well. The axial field measurements also agreed reasonably well with CST simulations [38]. The peak values measured in the low- and mid-field experiments were 3.5 ± 2.1 T and 11.5 ± 5.3 T, respectively. Unfortunately, the probe failed on the only high-field shot.

To study the instability evolution, a 12-frame visible self-emission imaging diagnostic and a 4-frame extreme ultraviolet (XUV) self-emission imaging diagnostic were fielded. The visible system used optical lenses coupled to an Invisible Vision Ultra UHSi intensified charge-coupled device (ICCD), while the XUV system used four 200-μm-diameter pinholes coupled to four micro-channel plates. Example images from both the SZP-driven experiments and the DSP-driven experiments are presented in Fig. 3. These images reveal the profound effects that the various return-current structures had on the instability evolution—in particular, helical modes were present for the DSP cases while azimuthally symmetric modes were present for the SZP case (the differing mode structures are more readily apparent in the XUV images). These observations are reminiscent of the helical striations observed on the surfaces of *non*imploding liners in experiments with twisted return-current structures [39].

The imploding helical structures presented in Fig. 3 can be described by their pitch angle $\phi_{\mathrm{plasma}}(t) \approx \arctan\{p/[2\pi r_\ell(t)]\} \approx m/[k_z r_\ell(t)]$, where p is the pitch and k_z is the axial wave number [20,23,32]. Importantly, as these helical structures implode, p and m/k_z are preserved, since axial outflows are not permitted. This allows us to trace $\phi_{\mathrm{plasma}}(t)$ back to the time when the liner first began to implode. This initial plasma pitch angle, $\phi_{\mathrm{plasma},0}$, can then be compared to the initial pitch angle of the driving magnetic field, $\phi_{B,0} = \arctan(B_z/B_\theta)$, which should have been constant up until the time when the liner started to implode. For example, in the XUV images of Fig. 3(c), $m/k_z = 22.5 \pm 2$ degree-mm, which traces back to $\phi_{\mathrm{plasma},0} = 7.0 \pm 0.7°$, while $\phi_{B,0} = 5.8 \pm 1°$. These initial pitch angles are nearly equal (within uncertainties), implying that the observed $\phi_{\mathrm{plasma}}(t)$ is set by $\phi_{B,0}$. The seeding mechanism likely involves the excitation of ETI and ECI at an angle consistent with $\phi_{B,0}$. Furthermore, since $\phi_{\mathrm{plasma}}(t)$ increases throughout the implosion, while $\phi_B(t)$ decreases throughout the implosion, $\mathbf{k} \cdot \mathbf{B} \neq 0$ for these most dominant helical structures, which should imply enhanced stability.

To quantify the stability of the implosions, the visible imaging data were analyzed to extract the instability amplitude as a function of the liner's normalized distance moved, $\hat{d} \equiv 1 - r_\ell(t)/r_\ell(0)$. The results of this analysis are presented in Fig. 4, where the instability amplitudes for the mid-field and high-field DSP cases are shown to be smaller than in the SZP case. Specifically, at $\hat{d} = 0.5$ ($C_r = 2$), the amplitudes for the SZP case and for the 14-T and 20-T DSP cases are, respectively, 1.1 ± 0.3 mm, 0.7 ± 0.2 mm, and 0.3 ± 0.1 mm. These amplitudes were found by tracking the plasma-vacuum interface and taking the difference between the peaks and valleys. The error bars represent the standard deviations in the measurements. We note that there was one low-field shot that appears to have

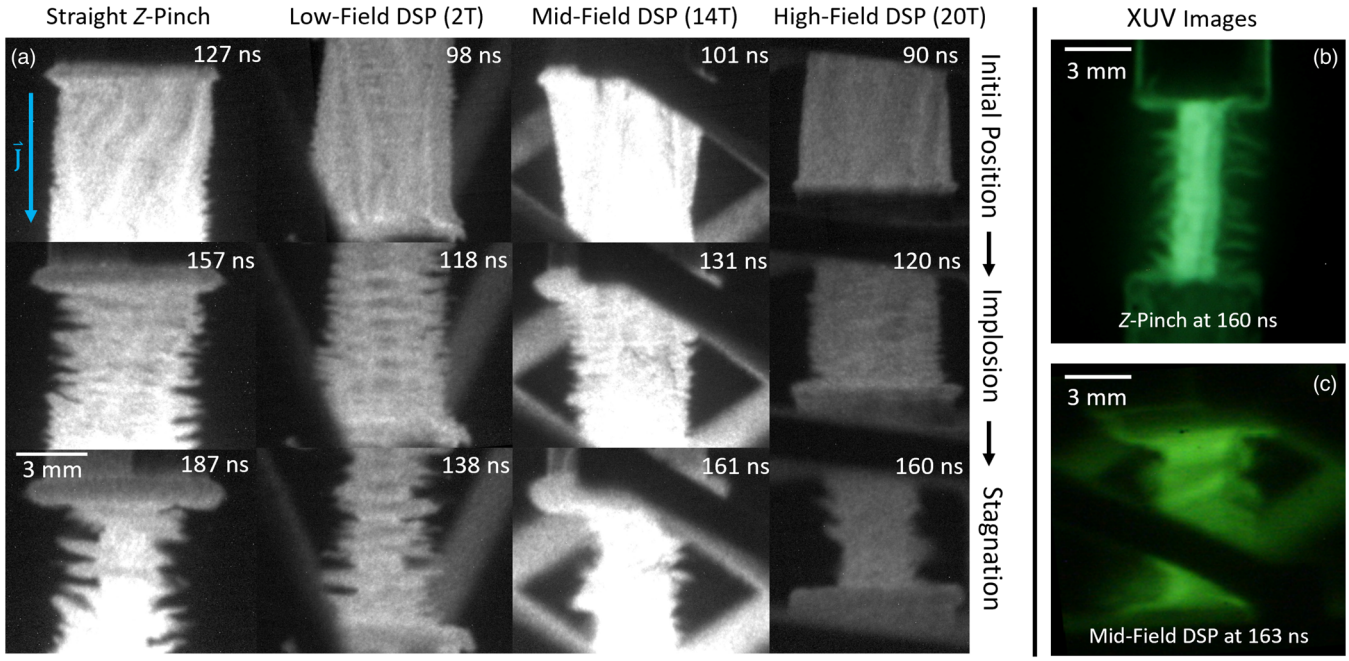

FIG. 3. (a) Visible self-emission images for each of the four experimental cases tested. (b) XUV image from a SZP experiment near stagnation. (c) XUV image from a mid-field DSP experiment near stagnation.

grown from a large initial perturbation, which is not surprising given the delicate nature of such thin-foil liners.

The overall implosion convergence observed for the liner's outer surface in these experiments ($C_r = 2$) is relatively small—e.g., the MagLIF program is interested in maintaining stability up to $C_r \approx 4$–10 (for the liner's outer surface). However, the relative stabilization obtained using the DSP configurations is only expected to increase with further increases to C_r and $\hat{d}$ [40]. Furthermore, the trends in the data are clear—increasing the B_z/B_θ ratio decreases the instability amplitude growth.

To compare the measured instability growth with theory, we used the finite-thickness cylindrical shell model of Ref. [41], which is based on linear perturbation analysis and includes Bell-Plesset effects. (Note that this model was also used in Ref. [28].) We used this model to calculate the amplitude growth for a dominant perturbation structure with a pitch angle that rotates according to our experimentally observed $\phi_{\text{plasma}}(t)$. This perturbation was driven by the experimental magnetic field, with a pitch angle that rotates according to $\phi_B(t)$. The perturbation was also allowed to cascade from shorter wavelengths to longer wavelengths, with $\lambda \propto \hat{d}$, as observed in our experiments and others [24]. This means that k_z as well as m cascade from larger values to smaller values, since $m/k_z \approx$ constant for imploding helical structures with constant pitch p. Based on our imaging data for $\hat{d} = 0.5$, we set the final axial wavelengths (λ_{zf}) for the SZP case and for the 2-T, 14-T, and 20-T DSP cases to 1 mm, 1 mm, 1.25 mm, and 1.5 mm, respectively. Since we do not know the initial perturbation wavelengths or amplitudes, we used the smallest wavelength observed to maintain a dominant (coherent) perturbation structure (50 μm) [17], and we used the initial amplitude (0.1 μm) that resulted in a match between theory and experiment for the amplitude growth of the SZP case at $\hat{d} = 0.5$. We then applied these same initial wavelength and amplitude values to the DSP cases to evaluate the relative stabilization. At $\hat{d} = 0.5$, the resulting amplitudes for the SZP case and for the 2-T, 14-T, and 20-T DSP cases were, respectively, 1.1 mm (by construction), 1.1 mm (i.e., no significant stabilization), 0.55 mm, and 0.33 mm. These results agree well with the results presented in Fig. 4; however, we caution that these results

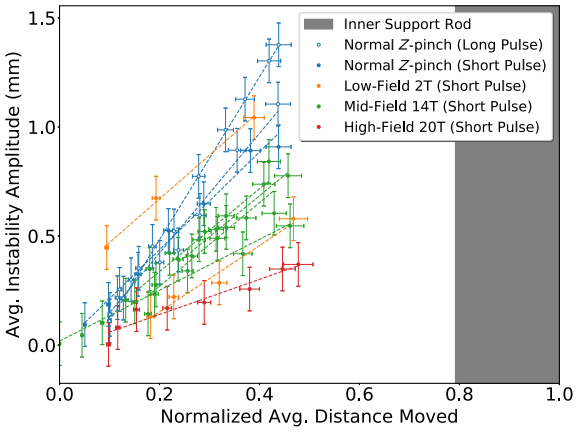

FIG. 4. A plot of the average instability amplitudes as a function of the normalized distance moved, $\hat{d} \equiv 1 - r_\ell(t)/r_\ell(0)$. Linear fits for each shot are plotted as dashed lines.

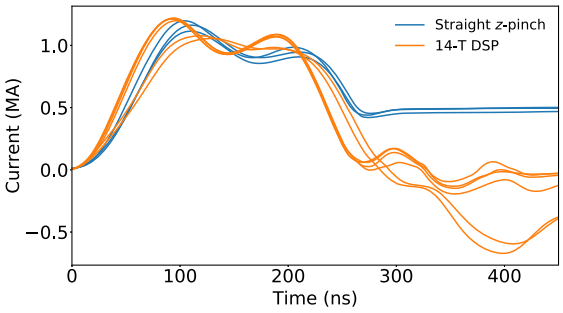

FIG. 5. Several SZP and mid-field DSP drive currents from the shot series. These plots illustrate the effects that the DSP configuration has on late-time load-current measurements and possibly on power flow after peak current.

depend on the λ_{zf} values chosen and on the shell thickness chosen (for which we used 250 μm, based on the exploding thin-foil studies presented in Refs. [33,34]). Moreover, we are using a linear perturbation theory to describe a fundamentally nonlinear process (i.e., a wavelength cascade due to mode merger events). To model these nonlinear experiments more appropriately, 3D MHD simulations like those presented in Ref. [40] are required. Such studies will be presented in a future publication.

Regarding power coupling, we note that when comparing across similar current pulses (e.g., considering only short pulse shots), the DSP cases often stagnated 20–40 ns earlier than the SZP cases (see Fig. 2). Simple thin-shell implosion modeling (0D) indicates that shot-to-shot variations in current delivery (∼10%) can only account for about 10–20 ns of variation in stagnation times. Thus, these earlier stagnation times are consistent with increased power coupling, as predicted in Refs. [28,29].

A second power flow observation is presented in Fig. 5. For the SZP case, the Rogowski coil appears to short out (or become shielded by plasma) around 300 ns (as indicated by these time-integrated signals not returning to zero). One explanation of this behavior [42–45] is that power flow and low-density plasma flow change direction with voltage reversal (and thus with the reversal of the electric field $\mathbf{E}$), which occurs after peak current in these pulsed inductive systems. In the SZP case, the $\mathbf{E} \times \mathbf{B}$ direction after peak current is away from the imploding liner. This drives low-density liner plasma back towards the Rogowski coil, which is located in the power feed a few cm away from the liner. In most of the DSP experiments, however, the Rogowski coil continues to measure the drive current for the duration of the pulse. This may indicate that the DSP configuration prevents low-density liner plasma from moving out into the power feed towards the Rogowski coil. Particle-in-cell simulations support this claim, indicating that after voltage reversal, electrons in the SZP case are directed back into the power feed, while electrons in the DSP cases are ejected radially outward through the gaps between the twisted return-current posts. These simulation results will be presented in a future publication.

The authors would like to thank Sophia Rocco, Jacob Banasek, Harry Wilhelm, Todd Blanchard, and Daniel Hawkes for their assistance with these experiments and Dr. Alexander (Sasha) Velikovich for helpful discussions on the theoretical interpretation of the results. This work was supported by the National Science Foundation under Grant No. PHY-1705418 of the NSF-DOE Partnership in Basic Plasma Science and Engineering. Facility support for COBRA was provided by the NNSA Stewardship Sciences Academic Programs under DOE Cooperative Agreement DE-NA-0003764. Sandia National Laboratories is a multimission laboratory managed and operated by National Technology and Engineering Solutions of Sandia, LLC., a wholly owned subsidiary of Honeywell International, Inc., for the U.S. Department of Energy's National Nuclear Security Administration under Contract No. DE-NA-0003525.

[1] D. D. Ryutov, M. S. Derzon, and M. K. Matzen, Rev. Mod. Phys. **72**, 167 (2000).
[2] M. G. Haines, Plasma Phys. Controlled Fusion **53**, 093001 (2011).
[3] G. A. Rochau, J. E. Bailey, G. A. Chandler, G. Cooper, G. S. Dunham, P. W. Lake, R. J. Leeper, R. W. Lemke, T. A. Mehlhorn, A. Nikroo, K. J. Peterson, C. L. Ruiz, D. G. Schroen, S. A. Slutz, D. Steinman, W. A. Stygar, and W. Varnum, Plasma Phys. Controlled Fusion **49**, B591 (2007).
[4] D. J. Ampleford *et al.*, Phys. Plasmas **21**, 056708 (2014).
[5] M. R. Martin, R. W. Lemke, R. D. McBride, J. P. Davis, D. H. Dolan, M. D. Knudson, K. R. Cochrane, D. B. Sinars, I. C. Smith, M. Savage, W. A. Stygar, K. Killebrew, D. G. Flicker, and M. C. Herrmann, Phys. Plasmas **19**, 056310 (2012).
[6] R. W. Lemke, D. H. Dolan, D. G. Dalton, J. L. Brown, K. Tomlinson, G. R. Robertson, M. D. Knudson, E. Harding, A. E. Mattsson, J. H. Carpenter, R. R. Drake, K. Cochrane, B. E. Blue, A. C. Robinson, and T. R. Mattsson, J. Appl. Phys. **119**, 015904 (2016).
[7] G. A. Rochau, J. E. Bailey, R. E. Falcon, G. P. Loisel, T. Nagayama, R. C. Mancini, I. Hall, D. E. Winget, M. H. Montgomery, and D. A. Liedahl, Phys. Plasmas **21**, 056308 (2014).
[8] J. E. Bailey *et al.*, Nature (London) **517**, 56 (2015).
[9] S. A. Slutz, M. C. Herrmann, R. A. Vesey, A. B. Sefkow, D. B. Sinars, D. C. Rovang, K. J. Peterson, and M. E. Cuneo, Phys. Plasmas **17**, 056303 (2010).
[10] S. A. Slutz and R. A. Vesey, Phys. Rev. Lett. **108**, 025003 (2012).
[11] M. E. Cuneo *et al.*, IEEE Trans. Plasma Sci. **40**, 3222 (2012).
[12] M. R. Gomez *et al.*, Phys. Rev. Lett. **113**, 155003 (2014).
[13] E. G. Harris, Phys. Fluids **5**, 1057 (1962).
[14] E. Ott, Phys. Rev. Lett. **29**, 1429 (1972).

[15] R. E. Reinovsky, W. E. Anderson, W. L. Atchison, C. E. Ekdahl, R. J. Faehl, I. R. Lindemuth, D. V. Morgan, M. Murillo, J. L. Stokes, and J. S. Shlachter, IEEE Trans. Plasma Sci. **30**, 1764 (2002).
[16] A. R. Miles, Phys. Plasmas **16**, 032702 (2009).
[17] D. B. Sinars *et al.*, Phys. Rev. Lett. **105**, 185001 (2010).
[18] Y. Y. Lau, J. C. Zier, I. M. Rittersdorf, M. R. Weis, and R. M. Gilgenbach, Phys. Rev. E **83**, 066405 (2011).
[19] P. Zhang, Y. Y. Lau, I. M. Rittersdorf, M. R. Weis, R. M. Gilgenbach, D. Chalenski, and S. A. Slutz, Phys. Plasmas **19**, 022703 (2012).
[20] M. R. Weis, P. Zhang, Y. Y. Lau, P. F. Schmit, K. J. Peterson, M. Hess, and R. M. Gilgenbach, Phys. Plasmas **22**, 032706 (2015).
[21] R. D. McBride *et al.*, Phys. Plasmas **20**, 056309 (2013).
[22] P. F. Schmit *et al.*, Phys. Rev. Lett. **113**, 155004 (2014).
[23] T. J. Awe *et al.*, Phys. Rev. Lett. **111**, 235005 (2013).
[24] R. D. McBride, Phys. Rev. Lett. **109**, 135004 (2012).
[25] K. J. Peterson, T. J. Awe, E. P. Yu, D. B. Sinars, E. S. Field, M. E. Cuneo, M. C. Herrmann, M. Savage, D. Schroen, K. Tomlinson, and C. Nakhleh, Phys. Rev. Lett. **112**, 135002 (2014).
[26] T. J. Awe, K. J. Peterson, E. P. Yu, R. D. McBride, D. B. Sinars, M. R. Gomez, C. A. Jennings, M. R. Martin, S. E. Rosenthal, D. G. Schroen, A. B. Sefkow, S. A. Slutz, K. Tomlinson, and R. A. Vesey, Phys. Rev. Lett. **116**, 065001 (2016).
[27] J. D. Pecover and J. P. Chittenden, Phys. Plasmas **22**, 102701 (2015).
[28] P. F. Schmit, A. L. Velikovich, R. D. McBride, and G. K. Robertson, Phys. Rev. Lett. **117**, 205001 (2016).
[29] S. A. Sorokin, Plasma Phys. Rep. **39**, 139 (2013).
[30] P.-A. Gourdain, M. B. Adams, J. R. Davies, and C. E. Seyler, Phys. Plasmas **24**, 102712 (2017).
[31] D. A. Yager-Elorriaga, P. Zhang, A. M. Steiner, N. M. Jordan, P. C. Campbell, Y. Y. Lau, and R. M. Gilgenbach, Phys. Plasmas **23**, 124502 (2016).
[32] D. A. Yager-Elorriaga, Y. Y. Lau, P. Zhang, P. C. Campbell, A. M. Steiner, N. M. Jordan, R. D. McBride, and R. M. Gilgenbach, Phys. Plasmas **25**, 056307 (2018).
[33] J. C. Zier, R. M. Gilgenbach, D. A. Chalenski, Y. Y. Lau, D. M. French, M. R. Gomez, S. G. Patel, I. M. Rittersdorf, A. M. Steiner, M. Weis, P. Zhang, M. Mazarakis, M. E. Cuneo, and M. Lopez, Phys. Plasmas **19**, 032701 (2012).
[34] M. R. Weis, Magneto-Rayleigh-Taylor instability: Theory and simulation in planar and cylindrical pulsed power targets, Ph.D. Thesis, University of Michigan, 2015.
[35] J. B. Greenly, J. D. Douglas, D. A. Hammer, B. R. Kusse, S. C. Glidden, and H. D. Sanders, Rev. Sci. Instrum. **79**, 073501 (2008).
[36] D. A. Yager-Elorriaga, A. M. Steiner, S. G. Patel, N. M. Jordan, Y. Y. Lau, and R. M. Gilgenbach, Rev. Sci. Instrum. **86**, 113506 (2015).
[37] J. Greenly, M. Martin, I. Blesener, D. Chalenski, P. Knapp, and R. McBride, AIP Conf. Proc. **1088**, 53 (2009).
[38] https://www.cst.com/products/cstems.
[39] L. Atoyan, D. A. Hammer, B. R. Kusse, T. Byvank, A. D. Cahill, J. B. Greenly, S. A. Pikuz, and T. A. Shelkovenko, Phys. Plasmas **23**, 022708 (2016).
[40] G. A. Shipley, C. A. Jennings, and P. F. Schmit, Phys. Plasmas **26**, 102702 (2019).
[41] A. L. Velikovich and P. F. Schmit, Phys. Plasmas **22**, 122711 (2015).
[42] M. G. Haines, Proc. Phys. Soc. **74**, 576 (1959).
[43] J. Greenly, C. Seyler, and X. Zhao, Bull. Am. Phys. Soc. **59**, 133 (2014), http://flux.aps.org/meetings/YR14/DPP14/all_DPP14.pdf.
[44] P. C. Campbell, J. M. Woolstrum, F. Antoulinakis, T. M. Jones, D. A. Yager-Elorriaga, S. M. Miller, N. M. Jordan, Y. Y. Lau, R. M. Gilgenbach, and R. D. Mcbride, IEEE Trans. Plasma Sci. **46**, 3973 (2018).
[45] R. D. McBride *et al.*, IEEE Trans. Plasma Sci. **46**, 3928 (2018).